JOURNAL OF GEOPHYSICAL RESEARCH, VOL. 104, NO. D17, PAGES 21,275–21,285, SEPTEMBER 20, 1999

Water content and morphology of sodium chloride aerosol particles

David D. Weis[1] and George E. Ewing
Department of Chemistry, Indiana University, Bloomington

Abstract. Sodium chloride droplets with a median diameter of ~0.4 μm were generated in the laboratory by atomizing an aqueous solution of NaCl under ambient conditions. Infrared extinction spectra of the aerosols under controlled relative humidity (RH) ranging from 15 to 95% were obtained. The extinction spectra contained both scattering and absorption components. In order to obtain an absorption spectrum of the condensed phase H_2O associated with the particulates, it was necessary to subtract from the extinction spectra the absorption by H_2O vapor and the scattering by the particulates. H_2O vapor subtraction was accomplished by a standard technique. A procedure using Mie theory to subtract the scattering component of the extinction spectrum is described. The absorption spectra were used to determine the water content and structure of the particulates. Above ~50% RH the aerosols contain aqueous droplets that have not reached equilibrium with the water vapor during the timescale of the experiments (~10 s). There is a sharp transition in water content at around 50% RH which is consistent with other measures of the recrystallization point. Below 50% RH the NaCl particles contain an anomalously large amount of H_2O. Several different particle models are considered to explain the H_2O content. The model in which the NaCl particles contain pockets of aqueous NaCl solution was found to be most consistent with the spectroscopic observations. The relevance of salt particle morphology and water content to atmospheric aerosol chemistry is discussed.

1. Introduction

Sodium chloride, as the principal component of sea salt, is a significant fraction of the total atmospheric particulate mass [*Warneck*, 1988]. It is estimated that $\sim 10^{12}$ kg of sea salt are injected into the atmosphere each year, primarily by wave action on the Earth's oceans [*Warneck*, 1988]. These particles begin their existence as droplets of seawater with diameters of 0.1–100 μm. Depending on the temperature and vapor pressure of water, these droplets may become more or less concentrated, or they may crystallize.

Solid sodium chloride is known to participate in a variety of heterogeneous chemical reactions such as (R1) [*Beichert and Finlayson-Pitts*, 1996; *Peters and Ewing*, 1996; *Robbins et al.*, 1959; *Vogt and Finlayson-Pitts*, 1994], (R2) [*Fenter*, 1996], (R3) [*Timonen et al.*, 1994], and (R4) [*Allen et al.*, 1996; *Davies and Cox*, 1998; *Horn et al.*, 1994; *Vogt and Finlayson-Pitts*, 1994]:

(R1) $2NO_2(g) + NaCl(s) \rightarrow NaNO_3(s) + ClNO(g)$

(R2) $N_2O_5(g) + NaCl(s) \rightarrow NaNO_3(s) + ClNO_2(g)$

(R3) $ClONO_2(g) + NaCl(s) \rightarrow NaNO_3(s) + Cl_2(g)$

(R4) $HNO_3(g) + NaCl(s) \rightarrow NaNO_3(s) + HCl(g)$

In each of these reactions, NaCl is converted to $NaNO_3$ with the concomitant release of chlorine. Photolysis of any of the chlorine-containing molecules from (R1) to (R3) may produce Cl radicals, which are powerful oxidants in the troposphere. There have been many laboratory studies of the kinetics of these reactions, particularly of (R1) and (R4), often with conflicting results. It appears that water plays a crucial role in the reaction and that the various methods that were used to prepare NaCl substrates described in the references above yield varying amounts of water. Thus it is crucial to understand how water interacts with salt particles that closely mimic those found in the atmosphere.

While it is reasonable to expect that aqueous seawater droplets will be homogeneous spheres when at equilibrium with the surrounding H_2O vapor, the morphology of the crystalline particles is less certain. One can rationalize many different structures, some of which are represented in Figure 1. They range from nonporous solids (I) to liquid droplets (which may be supersaturated) (VI) and various intermediate structures (II–V). The representations imply that water may remain associated with the particles, either as a thin adsorbed layer on the surfaces of the salt particle [*Barraclough and Hall*, 1974; *Bruch et al.*, 1995; *Dai et al.*, 1995; *Ewing and Peters*, 1997; *Fölsch and Henzler*, 1991; *Fölsch et al.*, 1992; *Foster and Ewing*, 1999; *Peters and Ewing*, 1997a, b; *Taylor et al.*, 1997; *Wasserman et al.*, 1993] (I and II) or as a bulk aqueous solution (III–VI). Particles containing bulk solution may be further divided into those for which the solution is exposed to the surrounding gases (III and V) and those for which the solution is trapped in the salt matrix (IV). Furthermore, the particles are not restricted to the six representations shown in Figure 1; they might be hybrids of two or more of the proposed structures.

According to homogeneous nucleation theory [*Cohen et al.*, 1987], which describes the crystallization from a supersatu-

[1]Now at Department of Chemistry and Biochemistry, Middlebury College, Middlebury, Vermont.

Paper number 1999JD900286.
0148-0227/99/1999JD900286$09.00

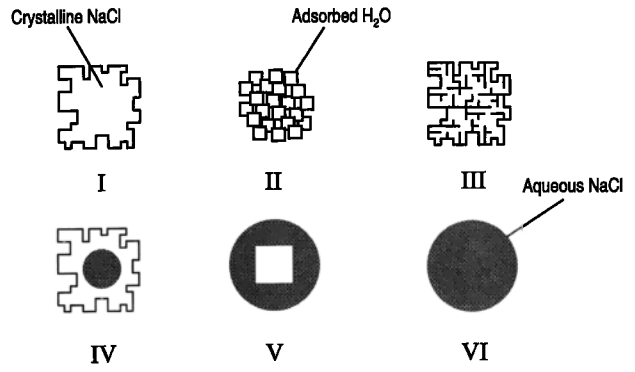

Figure 1. Possible structures for NaCl particles: (I) nonporous solid, (II) porous solid, (III) solid with open pockets of aqueous NaCl, (IV) solid shell with an aqueous NaCl core, (V) solid NaCl with aqueous NaCl shell, and (VI) aqueous droplet. The lines defining the boundaries of crystalline NaCl structures in I–IV are meant to represent thin films of adsorbed water.

rated solution, nucleation is preceded by the formation of one or more critical clusters. Once these clusters form, nucleation proceeds spontaneously. Depending on the size and concentration of the droplet, single or multiple nuclei may form inside a single droplet [*Leong*, 1987]. These possibilities would lead to the formation of structure I for single nucleus formation and structures II and III in the case of the formation of multiple nuclei [*Leong*, 1987]. Leong has argued that structure IV is most likely because evaporation occurs at the surface leading to increased solute concentration near the surface. This in turn results in crystallization at the surface and the formation of a solid shell around the droplet [*Leong*, 1987]. Structure V might be expected as an intermediate in the formation of structures I, II, and III. If there is insufficient time for crystallization to occur or the droplet is not concentrated enough, then structure VI might result.

Direct measurement of the shape of submicron particles requires collection on a support and analysis with electron microscopy. Both the support and the high vacuum of the electron microscope can induce significant changes in the structure and water content of a particle, the former by providing a heterogeneous surface to induce crystallization, the latter by causing liquid droplets to rapidly evaporate. Nevertheless, there are several electron micrographs of dried droplets of sea salt and sodium chloride which show that these particles form spheroidal aggregates of smaller cubic crystals [*Cheng*, 1988; *Liu*, 1976; *Pinnick and Auvermann*, 1979] resembling structure II, while others show the particles to be hollow spheres with a single, prominent pore [*Cheng et al.*, 1988]. There is at least one micrograph of furnace-dried sodium chloride droplets which shows that the particles form cubic particles [*Perry et al.*, 1978] resembling structure I, although there are some uncertainties about the sample handling.

Clearly, what is needed is an in situ technique that can provide information about the structure and water content of the particles. While infrared (IR) spectroscopy of submicron salt particles is not a particularly good probe of morphology, it has been applied quite successfully to studies of the composition of aerosol particles [*Anthony et al.*, 1995; *Bertram et al.*, 1996; *Clapp et al.*, 1995; *Cziczo et al.*, 1997; *Mudd et al.*, 1982; *Weis and Ewing*, 1996, 1997] and to the study of the association of water with supported sodium chloride crystals and crystallites [*Dai et al.*, 1995; *Ewing and Peters*, 1997; *Foster and Ewing*, 1998; *Peters and Ewing*, 1997a, b]. In a recent IR spectroscopic study of the crystallization and deliquescence of NaCl aerosol [*Cziczo et al.*, 1997], solid NaCl aerosol particles were found to retain a measurable amount of H_2O down to 4% RH. Cziczo et al. argued that this H_2O was physically trapped rather than adsorbed both because the signal was too large to be attributed to adsorbed H_2O and because there was no evidence of deuterium exchange when the particles were exposed to D_2O vapor. The goal of this paper is to extend the work of Cziczo et al. on NaCl aerosols by answering the following questions:

1. How much water is associated with the NaCl particles?
2. How does the water content depend on the relative humidity?
3. In what form is the water (pure liquid, aqueous solution, adsorbed, hydrate)?
4. Which of the structures in Figure 1 are consistent with the observations?

2. Experiment

A schematic of the experimental apparatus is shown in Figure 2. A solution of NaCl (SigmaUltra grade, >99.5%) in water (Alfa Aesar ultrapure spectrophotometric grade) with a concentration c of 0.20 kg of solute per liter of solution (3.4 M) was atomized into submicron droplets using a constant output atomizer (model 3076, TSI Inc.) driven by 240 kPa of N_2 (UHP/Zero grade, Air Products). The manufacturer specifies that the atomizer produces a lognormal distribution [*Hinds*, 1982] of particle diameters with a median diameter $\bar{d}$ of 0.35 μm, a geometric standard deviation ζ of 2, and a particle number density D_{part} of $\sim 10^{14}$ particles m^{-3}. In experiments in which a low relative humidity (<50% RH) was desired, the atomized solution passed through a diffusion dryer (model 3062, TSI Inc.) which consisted of a tube of wire cloth surrounded by silica gel desiccant. As the aerosol passes through the tube, H_2O vapor is adsorbed onto the silica gel. In experiments in which a high relative humidity (>45% RH) was desired, the diffusion dryer was bypassed, so the atomizer output went directly into the aerosol cell. The aerosol could be mixed with either dry or humidified N_2 at the mixing junction. The humidified N_2 was generated by bubbling N_2 through two coarse gas dispersion tubes (Ace Glassware) immersed in liquid water. The entire bubbler assembly was held at about 5°C above ambient temperature with a stirred temperature-controlled water bath. The ratio of humid to dry N_2 was controlled by adjusting the relative flow rates through two rotameters. The total flow rate of the two gas streams was held constant at $(7 \pm 1) \times 10^{-2}$ L s^{-1}. The NaCl aerosol was mixed with the N_2 stream, and the combined flow was directed through the IR cell. In some experiments, coiled tubing with an inner diameter of 1 cm and a length of up to 13 m was inserted between the mixing junction and the IR cell. This length of tubing increased the residence time of the aerosol particles from ~1 to ~10 s, permitting more time for the particles and gas to interact. The residence time was determined by measuring the time lag between the beginning of atomization and the arrival of the first particles in the cell. The latter was determined by directing a HeNe laser beam through the transparent tubing just upstream from the IR cell, as shown in Figure 2. The presence of the particles, as indicated by the scattering of the laser beam, was easy to observe by eye.

The aerosol cell, which was made of Pyrex, had an optical

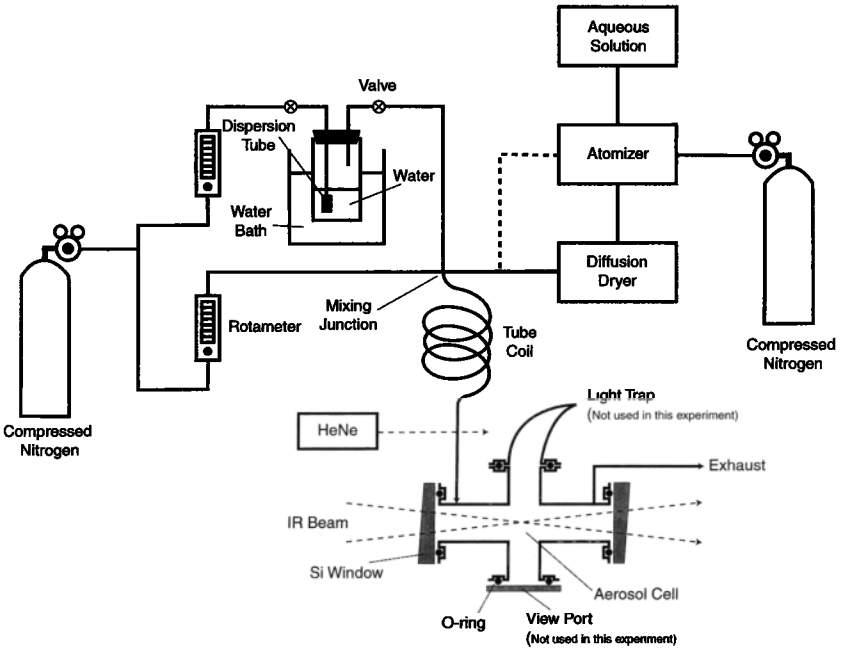

Figure 2. Schematic of the experimental apparatus. Wet aerosols (see section 2 for explanation) were obtained by bypassing the diffusion dryer (dashed line). The aerosol cell is 12 cm in length.

path length of 12 cm and an inside diameter of 2.5 cm. The ends were sealed with silicon windows having a 30 min wedge (Infrared Optical) to eliminate etalon fringes and vacuum grade O-rings held in place with standard clamps. The windows were not intentionally oriented either with respect to the cell or with each other. The cell was positioned in the sample compartment of the FTIR spectrometer such that the focus point of the IR beam was near the center of the cell. The laser window and light trap were also sealed to the cell with O-rings and clamps but were used for an experiment that is not reported here.

IR spectra were obtained with a Nicolet Magna 550 FTIR equipped with a mercury-cadmium-telluride (MCT) detector. The interferograms were recorded at 4 cm^{-1} resolution without zero filling and were triangle apodized prior to being fast Fourier transformed to obtain single-beam spectra. Extinction spectra $E(\tilde{\nu})$ were obtained from

$$E(\tilde{\nu}) = \log_{10}\left(\frac{I_0(\tilde{\nu})}{I(\tilde{\nu})}\right) \quad (1)$$

where $I_0(\tilde{\nu})$ is the background single-beam spectrum of the purged cell, and $I(\tilde{\nu})$ is the single-beam spectrum of the cell containing aerosol. The background spectrum was obtained by averaging 200 interferograms, while the aerosol spectrum was the average of 100 interferograms. As we shall discuss fully below, spectra of aerosols contain both absorption and scattering components, hence the use of the term extinction, as opposed to absorbance.

The percent relative humidity (% RH) of the aerosol was determined spectroscopically by measuring the integrated extinction of H_2O from 2000 to 1250 cm^{-1}. The percent relative humidity is given by

$$\%\mathrm{RH} = \frac{P_{H_2O}}{P^0_{H_2O}} \times 100\% \quad (2)$$

where P_{H_2O} is the pressure of H_2O, and $P^0_{H_2}O$ is the equilibrium vapor pressure of H_2O. A calibration curve of integrated extinction versus relative humidity was constructed by measuring the relative humidity of the gas stream in the absence of aerosol with a digital hygrometer (HI8564 Hanna Instruments). All measurements were taken at a total pressure of 1.1 ± 0.1 bar (consisting mostly of N_2) and a temperature of 23 ± 2°C. Because of the ±2°C uncertainty in the gas temperature, there was a ±15% uncertainty in $P^0_{H_2}O$ [*Linde*, 1998]. Since the temperature of the experimental system can be expected to remain constant within ±0.5°C or better, the ±15% uncertainty in relative humidity is systematic rather than random.

3. Results

To characterize the behavior of the system, tests were made using aerosols generated from an $(NH_4)_2SO_4$ solution with a concentration of 0.20 kg L^{-1}. $(NH_4)_2SO_4$ aerosols have a well-documented spectroscopy [*Weis and Ewing*, 1996, 1997] which allows determination of the solute mass concentration based on the absorption by the IR-active modes of the molecular ion. Under the same experimental conditions used for the NaCl experiments, the $(NH_4)_2SO_4$ optical measurements showed that the solute mass concentration of the aerosol was (1.1 ± 0.1) × 10^{-3} kg m^{-3} of cell volume for all tubing lengths and all humidities. Since the density and viscosity of the $(NH_4)_2SO_4$ solution are only 3 and 7% less than those of the NaCl solution [*Linde*, 1998], we can reasonably assume that atomization of the solutions will result in aerosols with the same size distribution and number density. Therefore we may take the NaCl solute concentration in the aerosol to be $[m_{NaCl}]$ = (1.1 ± 0.1) × 10^{-3} kg m^{-3} of cell volume. The $(NH_4)_2SO_4$ measurements also indicated that there was an insignificant accumulation of particulate material on the window surfaces; likewise, it is assumed that there was no loss of NaCl to the cell windows.

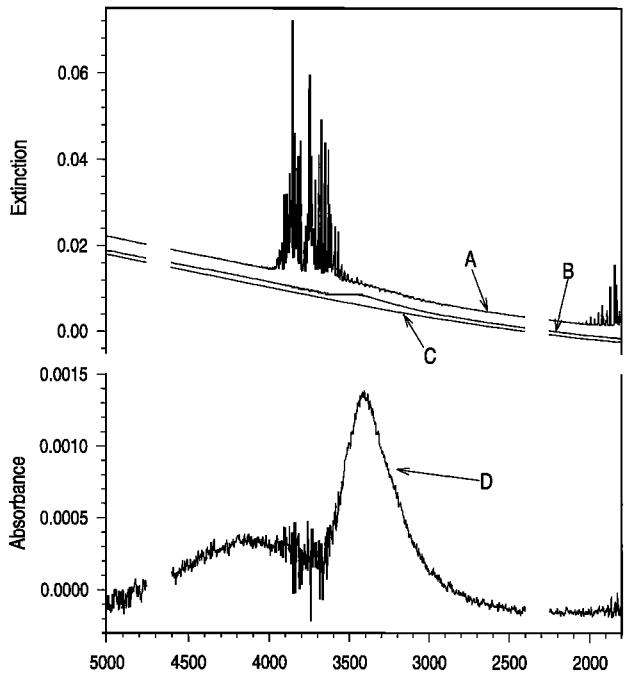

Figure 3. NaCl aerosol at 14 ± 2% RH: (curve A) the extinction spectrum, (curve B) after subtraction of H_2O vapor, (curve C) calculated scattering component. Curves B and C have been offset for clarity, (curve D) absorption spectrum obtained by the subtraction of curves C from B. Curve D is plotted on a different vertical scale. The spectral regions 4750–4600 cm^{-1} and 2400–2250 cm^{-1}, which contained features due to atmospheric CO_2, have been deleted.

Figure 3, curve A, shows the extinction spectrum of an NaCl aerosol at 14 ± 2% RH. The sharp features around 3900 and 1900 cm^{-1} are due to absorption by H_2O vapor. The 4750–4600 and 2400–2250 cm^{-1} regions, which encompass the well-characterized absorption by traces of CO_2, have been deleted. The only other readily apparent feature in the spectrum is the rise in the baseline with increasing wavenumber, which is a consequence of the scattering of light by the NaCl particles [*Bohren and Huffman*, 1983]. The interfering H_2O vapor signal can be dramatically reduced but not completely eliminated [*Weis and Ewing*, 1998] by the scaled subtraction of a spectrum of pure H_2O vapor. The FTIR software permits this subtraction to be done interactively by allowing the user to manually adjust the scaling factor until a minimum in the difference spectrum is found. The resulting spectrum (Figure 3, curve B) (which has been given a negative offset for clarity) contains extinction features that can be attributed to the aerosol particulates. In addition to the scattering component, an absorption component around 3400 cm^{-1} is now visible but is overwhelmed by the large scattering component. Using the program MIECALC [*Weis*, 1998; *Weis and Ewing*, 1996], the scattering component of the spectrum (Figure 3, curve C) (which has been given a negative offset for clarity) was calculated from Mie theory using the real index of refraction of solid NaCl [*Gray*, 1982]. Although Mie theory strictly applies only to spherical particles [*Bohren and Huffman*, 1983; *van de Hulst*, 1957], to a good approximation it reproduces the extinction spectrum of a collection of small, rotationally averaged nonspherical particles [*Perry et al.*, 1978]. The details of the calculation of the scattering component may be found in the Appendix.

The calculated scattering spectrum was subtracted from the experimental spectrum to produce the absorption spectrum shown in Figure 3, curve D. There are several absorption regions evident in Figure 3, curve D. The first is a diffuse absorption centered at 3403 ± 10 cm^{-1} with a full width at half maximum, Γ, of 360 ± 30 cm^{-1}. Later, this feature will be assigned to liquid water. The next region, ~3750 cm^{-1}, consists of series of sharp features due to the imperfect subtraction of H_2O vapor [*Weis and Ewing*, 1998] from Figure 3, curve A. The broadband at ~4100 cm^{-1} is an artifact of the subtraction of the scattering component. Its origin is a dip in the scattering spectrum on the high-wavenumber side of an absorption band possibly due to changes in the real component of the index of refraction of water in this region which were not included in the calculation. Thus the dip is not compensated for in the scattering calculation in Figure 3, curve C.

Figure 4, curve A, shows the extinction spectrum of an NaCl aerosol at 88 ± 13% RH after the interfering H_2O vapor features have been subtracted. Since the scattering and absorption components of the spectrum are comparable in size, an extinction spectrum (Figure 4, curve B) was fit to the experimental spectrum using the index of refraction of 5 M NaCl [*Querry et al.*, 1972], as described in the Appendix. The scattering component of the calculated extinction spectrum (Figure 4, curve C) was then subtracted from the experimental spectrum to yield the absorption spectrum (Figure 4, curve D), which has been offset for clarity. A single feature is evident in Figure 4, curve D, having a broad absorption centered at 3415 ± 10 cm^{-1}. This band has a full width at half maximum

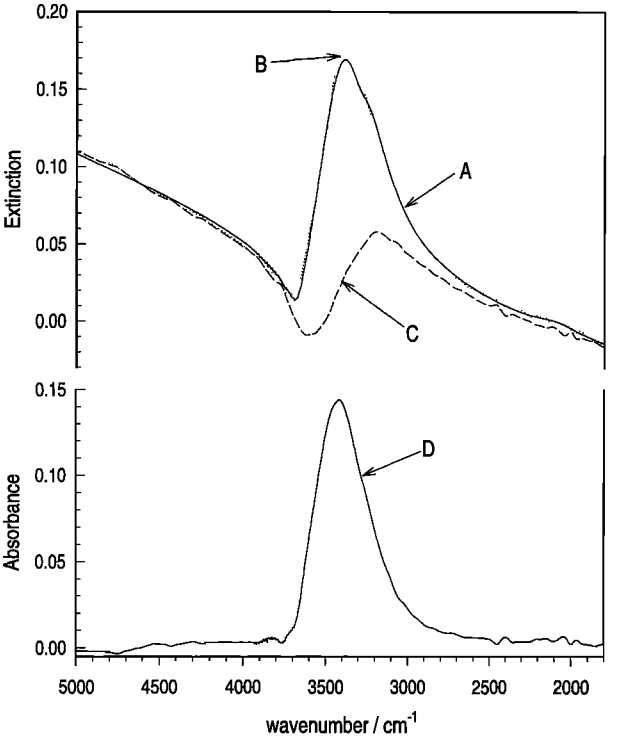

Figure 4. NaCl aerosol at 88 ± 13% RH: (curve A) the extinction spectrum after subtraction of H_2O vapor, (curve B) calculated extinction spectrum, (curve C) scattering component of B, (curve D) absorption spectrum obtained by the subtraction of curves C from A. Curve D is plotted on a different vertical scale.

of 390 ± 30 cm^{-1}. As in the case of Figure 3, curve D, this feature will be assigned to liquid water.

Figure 5 shows the integrated absorbance $\tilde{A}$ (3600–2800 cm^{-1}) of the prominent feature in the absorption spectra as a function of the relative humidity of the aerosol for two different types of aerosols: those that had passed through the diffusion dryer (solid circles) and those that had not (open circles). The NaCl aerosols below 43% RH have a small but easily measurable integrated absorbance, as shown in the insert. Above 48% RH the absorption is much stronger and increases with increasing RH.

Figure 6 shows the water absorption band center for the dried and wet NaCl aerosols (solid and open circles). The large estimated uncertainty of the band center (±10 cm^{-1}) in the aerosol spectra arises from the extensive processing required to obtain an absorption spectrum. The full width at half maximum of the water absorption band was 300 ± 50 cm^{-1} for all of the NaCl aerosol samples. Within the uncertainty limits, the band centers and bandwidth of the water band in the aerosol spectra are invariant with humidity.

Figure 7 shows the time dependence of the extinction by the water band for a diffusion-dried NaCl aerosol at 12 ± 2% RH (Figure 7a) and an NaCl aerosol at 44 ± 7% RH which was not diffusion dried (Figure 7b). The variation in the residence time was obtained by selecting different lengths of tubing of up to 13 m. For a given flow rate, the tube length and diameter determine the residence time of the aerosol in its dry or humid environment, as described in the experimental section. For the diffusion-dried aerosol the residence time could be varied between 3 and 9 s; for the more humid aerosol the residence time could be varied from 1 to 7 s. The longer residence time for the diffusion-dried aerosols arises from the inclusion of the diffusion dryer in the aerosol delivery system. In both sets of spectra, H_2O vapor has been subtracted, but the spectra have not been processed in any other way. Figure 7a shows that there is essentially no change (other than a slight drift in the baseline) in the absorption by the water band over the 6 s time interval of the experiment. By contrast, there is a significant decrease in the absorbance of the band of the more humid NaCl aerosol, with the band absorbance dropping by roughly a factor of 3 in 6 s.

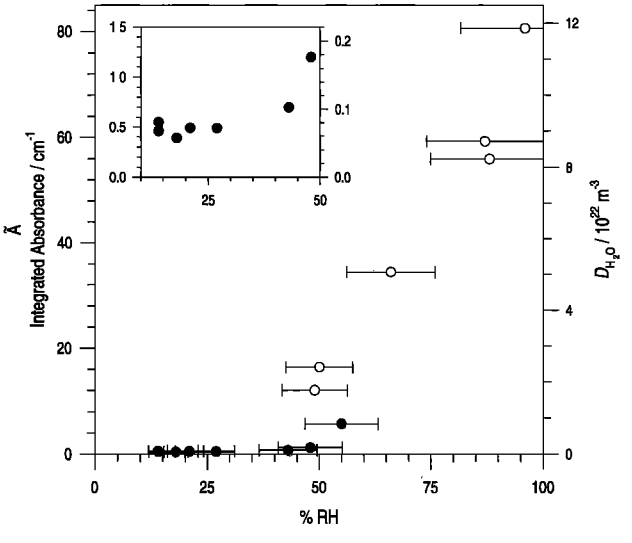

Figure 5. Integrated absorbance of the OH-stretching vibration band (left-hand side) and the concentration of liquid water molecules per m^{-3} of cell volume (right-hand side) as derived from the integrated absorbance. The plot shows measurements for both NaCl aerosols that were diffusion dried (solid circles) and those that were not (open circles). The inset shows the low relative humidity data with all axes having the same units as the main figure.

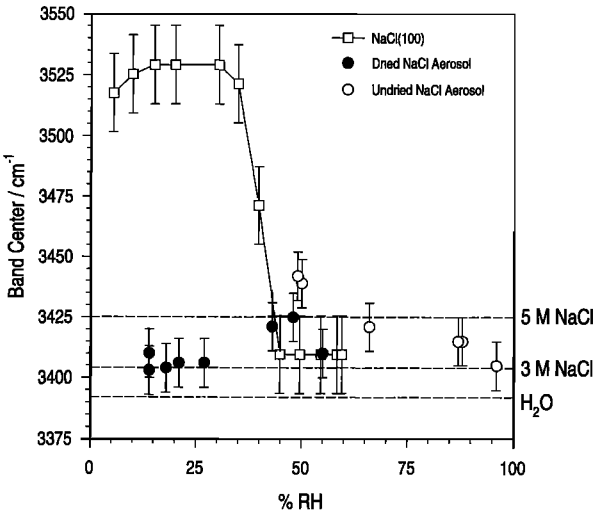

Figure 6. Band centers of the OH-stretching band as a function of relative humidity for diffusion-dried NaCl aerosols (solid circles) and undried aerosols (open circles). The band center for H_2O adsorbed on the (100) faces of NaCl single crystals at 30°C [*Foster and Ewing*, 1999] (open squares) is also shown. The horizontal dashed lines show the band center of the OH-stretching band for pure liquid H_2O [*Downing and Williams*, 1975] and for 3 M and 5 M NaCl solutions [*Querry et al.*, 1972].

4. Discussion

4.1. Infrared Water Signatures

The aerosol absorption band at 3400 cm^{-1} may be found in the IR spectrum of liquid water [*Downing and Williams*, 1975] and its aqueous NaCl solutions [*Querry et al.*, 1972] and has been assigned to the OH-stretching vibration of water. While there is a slight (~1%) variation in the band center with NaCl concentration, as the dashed horizontal lines in Figure 6 show, this diffuse feature, with bandwidth 300 ± 30 cm^{-1}, is taken to be the infrared signature for hydrogen-bonded liquid water. The corresponding absorption for H_2O adsorbed on the (100) faces of NaCl at 30°C on single crystals has some characteristic differences. Below 40% RH the band center is at 3525 cm^{-1} and remains invariant to humidity changes in this arid region, as shown on Figure 6. Here the coverage of adsorbed water is in the submonolayer region with a hydrogen-bonded network resembling strings [*Wasserman et al.*, 1993] or small two-dimensional islands [*Peters and Ewing*, 1997a, b]. The band center undergoes an abrupt frequency decrease to 3400 cm^{-1} above 50% RH and maintains this value toward the NaCl deliquescence point at 75% RH [*Tang and Munkelwitz*, 1991]. In this region the adlayer is described as liquid-like [*Foster and Ewing*, 1998; *Peters and Ewing*, 1997a, b] since its infrared signature resembles that of the bulk liquids, as shown in Figure 6. The OH-stretching vibration feature shows another distinctive signature for H_2O adsorbed on a sublimed NaCl film as described by *Dai et al.* [1995]. In these experiments, nanometer size crystallites, rich in defects, were exposed to H_2O at ~2% RH at 25°C, producing a submonolayer adlayer of H_2O on the NaCl surface, which revealed a quartet of features

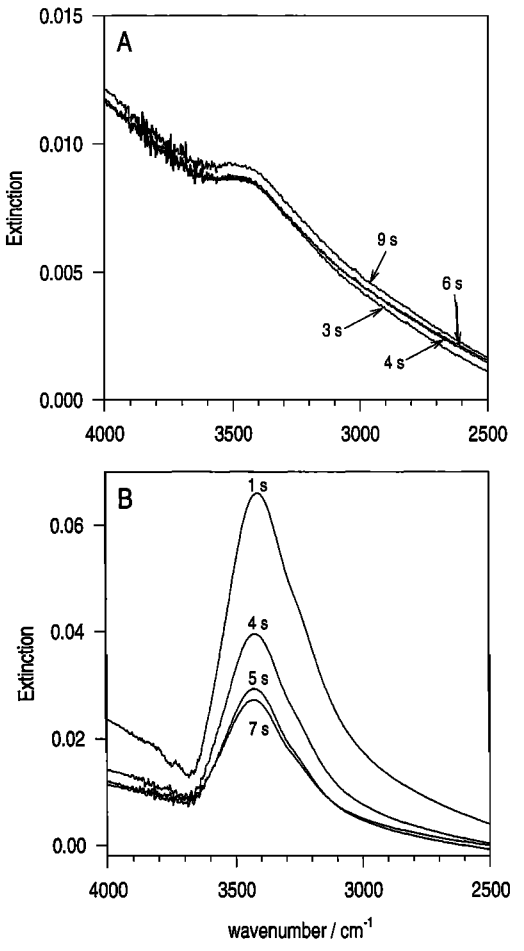

Figure 7. Extinction spectra (after H_2O vapor subtraction) of NaCl aerosols after various equilibration times. NaCl aerosols were maintained at (a) 12 ± 2% RH for 3, 4, 6, and 9 s and at (b) 44 ± 7% RH for 1, 4, 5, and 7 s.

(located at ~3400, 3500, 3650, and 3700 cm^{-1}) in the OH-stretching region. Presumably, water here is principally bonded to defects [*Dai et al.*, 1995; *Ewing and Peters*, 1997]. Increasing the water vapor pressure above this (exceedingly) arid level produced the characteristic absorption feature of brine (~3400 cm^{-1}) [*Querry et al.*, 1972].

As comparisons with Figure 6 demonstrate, the aerosol OH-stretching frequency is consistent with that of the aqueous solutions at all relative humidities regardless of whether or not the particles are dried. Similarly, the band shapes and bandwidths are consistent with aqueous NaCl at all humidities. Thus the spectroscopic signature of water associated with NaCl aerosol is consistent with bulk aqueous solution and inconsistent with the signatures of H_2O molecules adsorbed either on ordered or on disordered NaCl surfaces in the arid regions.

4.2. Quantitation of Water

The water content of the aerosol particles can be determined by using the Beer-Lambert law:

$$D_{H_2O} = \frac{2.303(10^2)\bar{A}}{\bar{\sigma}z} \tag{3}$$

where D_{H_2O} is number of water molecules per unit volume of the aerosol sample, z is the path length, and $\bar{\sigma}$ is the integrated absorption cross section per molecule. (The factor 10^2, which increases (3) by 2 orders of magnitude with respect to its conventional form, converts the integrated absorbance of $\bar{A}$ in cm^{-1} to SI units of m^{-1}.) For light passing through a homogeneous film of material with an imaginary index of refraction, κ, the integrated absorption cross section can be written as [*Bohren and Huffman*, 1983; *Weis and Ewing*, 1996]

$$\bar{\sigma} = \frac{4\pi 10^4}{p} \int_{band} \kappa\tilde{\nu}\, d\tilde{\nu} \tag{4}$$

where p is the molecular density of the bulk material (molecules m^{-3}) and the factor of 10^4 assures that (4) is in SI units. As in previous IR studies of H_2O-NaCl systems [*Peters and Ewing*, 1996a, b], κ for a 5M NaCl solution [*Querry et al.*, 1972] is used and gives $\bar{\sigma} = 1.3 \times 10^{-18}$ m molecule^{-1} for integration over the 2800–3600 cm^{-1} range. Using κ for pure H_2O [*Downing and Williams*, 1975] produces the same value for $\bar{\sigma}$, showing that absorption by liquid water in this spectral region is independent of the NaCl concentration. As discussed elsewhere [*Weis and Ewing*, 1996], for collections of particles that have small dimensions with respect to the wavelength of light passing through them, the absorption is nearly the same (±10%) for a given number of molecules dispersed in an aerosol as for the same number of molecules condensed into a bulk film. The results of this quantitation are shown in the right-hand side of Figure 5.

4.3. Water Content of NaCl Particles

The water content of NaCl particles exhibits a hysteresis effect as the relative humidity is changed much like that for $(NH_4)_2SO_4$ aerosols [*Tang et al.*, 1995]. As other studies of NaCl have shown [*Barraclough and Hall*, 1974; *Bruch et al.*, 1995; *Dai et al.*, 1995; *Ewing and Peters*, 1997; *Fölsch and Henzler*, 1991; *Fölsch et al.*, 1992; *Foster and Ewing*, 1999; *Peters and Ewing*, 1997a, b; *Taylor et al.*, 1997; *Wasserman et al.*, 1993], for crystalline particles, there is little change in the water content (except for a small amount of adsorption on the surface) as the relative humidity is increased, until the deliquescence point of 75% RH [*Tang and Munkelwitz*, 1991] is reached. At this point the particle rapidly takes up water and becomes a saturated droplet. However, these droplets do not recrystallize when the relative humidity falls below the deliquescence point. Instead, the particles become supersaturated, finally recrystallizing at 44% RH [*Cohen et al.*, 1987]. Thus NaCl particles below 44% RH can be expected to be crystalline regardless of how they were generated, and their water content must be explained in terms of entrainment in the particles or adsorption on the surfaces of the particles.

The invariance of the OH-stretching band extinction in Figure 7a indicates that aerosols at 12 ± 2% RH as well as those below 44% RH (the solid symbols in Figures 5 and 6), which were diffusion dried, have apparently reached equilibrium with H_2O vapor after only 3 s. Some aerosols (the open circles in Figures 5 and 6) were generated by bypassing the dryer. Figure 7b shows that there is a significant decrease in the water content of the NaCl particles at 44 ± 7% RH over a 6 s time period. This indicates that these undried particles are not in equilibrium with H_2O vapor at least at the early times (1–5 s). Since the relative humidity is less than that characterizing the deliquescence point, the equilibrium conditions require the droplets to be supersaturated, thus the loss of water is reason-

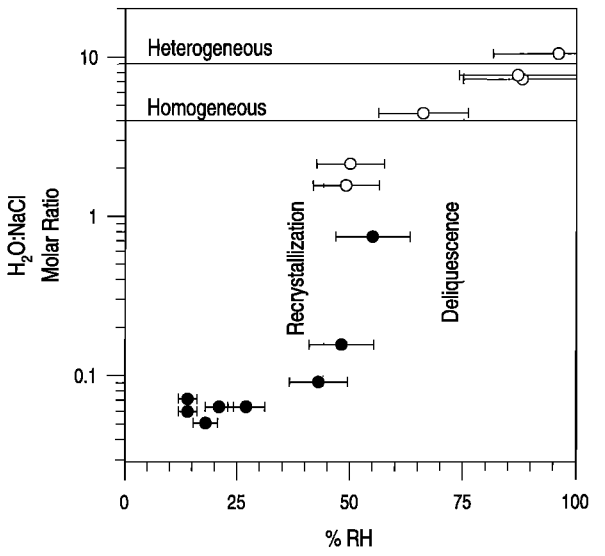

Figure 8. Water content of NaCl aerosols as a function of relative humidity for NaCl aerosols which passed through the diffusion dryer (solid circles) and those which did not (open circles). The left vertical axis gives the H_2O:NaCl molar ratio. The vertical reference lines show the deliquescence [*Tang and Munkelwitz*, 1991] and recrystallization points [*Cohen et al.*, 1987]. The horizontal reference lines show the H_2O:NaCl molar ratio at the heterogeneous (saturation) [*Linde*, 1998] and homogeneous nucleation (supersaturation) [*Cohen et al.*, 1987] limits.

able. All of the data shown in Figures 5–7 for NaCl aerosol that did not pass through the diffusion dryer were taken at short times of 1–2 s and thus cannot be expected to be at equilibrium. Below the deliquescence point, the measured water content is higher than would be expected for equilibrated particles, while above the deliquescence point, the measured water content is lower than would be expected at equilibrium. Even with this limitation, there is clearly a transition evident in Figure 5, with a significant change in water content occurring at around 50% RH, consistent with a previous IR spectroscopic study [*Cziczo et al.*, 1997]. Given the uncertainty in the relative humidity, this transition can be attributed to the crystallization of supersaturated droplets, which is expected at 44% RH [*Cohen et al.*, 1987]. Since it appears that the NaCl aerosols above 44% RH are not in equilibrium with H_2O vapor, the remainder of the discussion will deal primarily with the crystalline NaCl aerosols below 44% RH.

The ion pair concentration of NaCl per unit volume of aerosol sample, D_{NaCl}, is obtained from the solute mass concentration of the aerosol (1.1 ± 0.1) $\times 10^{-3}$ kg m^{-3} of cell volume to give $D_{NaCl} = (1.1 \pm 0.1) \times 10^{22}$ m^{-3}. The molar ratio H_2O:NaCl is then simply D_{H_2O}/D_{NaCl}. This ratio is plotted in Figure 8 as a function of relative humidity for the NaCl aerosols. Also shown are the maximum H_2O:NaCl molar ratios at the onset of heterogeneous [*Linde*, 1998] and homogeneous nucleation [*Cohen et al.*, 1987]. For the dried particles (solid circles) the ratio is always less than 1, which is well below the maximum supersaturation of 4.

4.4. Structure of NaCl Particles

In this section we will use the water content and the spectroscopic signature of the OH-stretching feature to distinguish among the various structures proposed in Figure 1. The conclusions that we will draw in this section depend heavily on our demonstrated ability to quantitatively determine D_{H_2O} and D_{NaCl}.

First, we will consider the possibility that the water observed at low humidity is due to H_2O adsorbed on NaCl surfaces. Assuming that all of the condensed phase water is adsorbed on the NaCl, the number of layers of H_2O adsorbed on the surface of NaCl, Θ, is given by

$$\Theta = \frac{D_{H_2O}}{[a_{NaCl}]S_{NaCl}} \tag{5}$$

where $[a_{NaCl}]$ is the particulate surface area per unit volume of aerosol (m^2 m^{-3}) and $S_{NaCl} = 6.4 \times 10^{18}$ m^{-2} is the surface density of Na^+Cl^- pairs [*Linde*, 1998]. A coverage of $\Theta = 1$ describes an NaCl surface for which, on average, each surface Na^+Cl^- pair has one H_2O molecule adsorbed to it.

The surface area $[a_{NaCl}]$ cannot be measured directly, but it may be estimated on the basis of a model of the particle morphology. First, we imagine that when a droplet of aqueous NaCl dries, it forms a single nonporous cube that retains all of the solute. This, then, is an examination of the feasibility of structure I in Figure 1 as a model for the NaCl particle morphology. In this case, the median cube edge length $\bar{s}$ is given by

$$\bar{s} = \sqrt[3]{\frac{\pi c}{6\rho}}\,\bar{d} \tag{6}$$

where c is the initial concentration of NaCl in the aqueous droplet (2.0×10^2 kg of solute per m^3 of solution) and ρ is the density of solid NaCl (2.2×10^3 kg m^{-3}) [*Linde*, 1998]. The manufacturer's specifications for the atomizer give $\bar{d} = 0.35$ μm, which yields $\bar{s} = 0.13$ μm. For a lognormal distribution of cubes with a median edge length of $\bar{s}$ and a geometric standard deviation of ζ, the particle number density D_{part} (particles m^{-3}) is given by

$$D_{part} = [m_{NaCl}]/\rho(\bar{s}\,\exp\,(\tfrac{3}{2}\ln^2\zeta))^3, \tag{7}$$

where $[m_{NaCl}]$ is the mass concentration of NaCl, 1.1×10^{-3} kg m^{-3} (see section 3). The quantity enclosed in the outer parentheses is a form of the Hatch-Choate equation that relates the median length to the mean mass [*Hinds*, 1982]. The number density is then 2.5×10^{13} m^{-3}. The surface area is given by

$$[a_{NaCl}] = D_{part}6(\bar{s}\,\exp\,(\ln^2\zeta))^2. \tag{8}$$

Again, the quantity enclosed by the outer set of parentheses is a form of the Hatch-Choate equation that relates median length to mean surface area [*Hinds*, 1982]. The resulting surface area is 6.6 m^2 m^{-3} of cell volume.

Armed with an estimate of the surface area of the particulates, we may calculate the coverage of H_2O, Θ, from (5) using the spectroscopically measured D_{H_2O} from (3). Below the recrystallization point of 44% RH [*Cohen et al.*, 1987], where the NaCl particles are crystalline, the mean coverage on the NaCl aerosol is $\Theta = 20 \pm 4$, roughly 2 orders of magnitude larger than the maximum observed coverage for H_2O adsorbed on single crystal NaCl [*Foster and Ewing*, 1998]. The calculation of Θ is based on the assumption of the manufacturer's specifications for the median diameter and geometric standard deviation. If a generously large uncertainty of a factor of 2 is applied to the median diameter, this factor may be propagated from

(6) to (8) to give an uncertainty of a factor of 2 in $[a_{NaCl}]$, which still does not account for the discrepancy between Θ for the NaCl aerosol and for NaCl(100) single crystals. A factor of 2 for the increase in surface area, which is implied by the corrugations on structure I in Figure 1, still demands a value of Θ which is too great. On the basis of these calculations we may confidently reject structure I for NaCl aerosols below 44% RH.

The failure of the nonporous cube model leads to two possibilities: first, that the assumption of nonporous cubes of NaCl is incorrect, or second, that water is present in inclusions. One way to increase the surface area of hypothetical NaCl particles is by forming aggregates of small uniform cubes with an edge length of s^*, as is represented by structure II, such that the total volume (or equivalently mass) of NaCl is held constant. As is shown in the Appendix, the total surface area per unit volume, $[a_{NaCl}]$ (m^2 m^{-3}), is then given by

$$[a_{NaCl}] = D_{part}6(\bar{s} \exp(\tfrac{3}{2} \ln^2 \zeta))^3 \frac{1}{s^*}. \quad (9)$$

From (9) the value of s^*, which is required to increase $[a_{NaCl}]$ by 2 orders of magnitude from 6.6 to 660 m^2 m^{-3}, is $s^* = 4$ nm. This would have the effect of reducing the observed coverage by 2 orders of magnitude, bringing it into agreement with the coverage values for H_2O on single-crystal NaCl(100) [*Foster and Ewing*, 1998]. Thus on the basis of the number of H_2O molecules, the observed value of below 44% RH is consistent with adsorption of H_2O on highly porous aggregates of 4 nm NaCl cubes.

While the anomalously large amount of condensed water may be justified by invoking adsorption on a highly porous substrate, the spectroscopic signature for water is not consistent with this interpretation. *Dai et al.* [1995] examined H_2O adsorbed on sublimed films of NaCl containing nanometer size crystals with a high concentration of defects. As was discussed in section 1, the OH-stretching band for H_2O adsorbed on the NaCl film is quite distinct from that of the water associated with NaCl aerosol. Furthermore, these films were found to deliquesce at very low humidity compared with bulk NaCl. The water signature is also inconsistent with adsorption on single crystal NaCl(100) under arid conditions, as shown in Figure 6. At any relative humidity the NaCl aerosol OH-stretching frequency is indistinguishable from that of concentrated NaCl solutions [*Querry et al.*, 1972]. On the basis of these lines of reasoning we may reject structure II in Figure 1 as a model for the NaCl particles below 44% RH.

Having dispensed with models of the NaCl particles below 44% RH, which attribute the observed to adsorption (structures I and II), we will now consider models that associate with the presence of bulk NaCl solution. On the basis of the near invariance of the band center and bandwidth of the OH-stretching mode and their consistency with concentrated aqueous NaCl solutions, the large amount of water observed must be due to the presence of NaCl solution such as represented in Figure 1 by structures III–VI.

For particles below 44% RH the H_2O:NaCl molar ratio is less than or equal to 0.1, while at the maximum observed supersaturation before the onset of homogeneous nucleation, the ratio was 4 [*Cohen et al.*, 1987]. On this basis, structure VI is discarded. The particles simply do not contain enough water to be homogeneous droplets of concentrated NaCl solution. While the small molar ratio does not exclude structure V, it would permit only a thin aqueous shell. Furthermore, the water content of structure V should depend strongly on the relative humidity in contrast to the result in Figure 8. At low humidity, structure V should not be stable. The shell of NaCl solution would evaporate leaving behind structure I, II, or III.

What remains, then, is the conclusion that water is present in pockets such as those represented by structures III or IV in Figure 1. While it is not easy to distinguish between these two models on the basis of the IR spectroscopy, electron micrographs of dried NaCl and sea-salt particles that have a structure similar to IV but also feature a prominent pore in the salt shell [*Cheng et al.*, 1988]. However, such a pore would permit the loss of water through evaporation, thereby reducing the water content. By contrast, water incorporated into structure III might not evaporate because of capillary effects associated with small fissures in an NaCl crystal or microscopic gaps between crystals in an aggregate. *Cziczo et al.* [1997] also observed a large water content for NaCl particles at low relative humidity using IR spectroscopy. Although they did not observe any IR absorption due to the OD stretching mode upon exposure of the particles to gas phase D_2O (as would be expected if H-D exchange occurred), this might seem to suggest that the water inclusions are not exposed to the gas phase. However, this result may also be explained by a capillary effect, since exchange between the gas phase and the fissures or gaps would be slow.

Whether structure III or IV forms may have great importance to the chemistry of sea-salt aerosol in the atmosphere. If structure III is favored, then heterogeneous chemistry may take place not just between gas and solid but may also involve gas-liquid and liquid-solid reactions. (Tropospheric processes involving sea-salt aerosol operate on the timescale of days, whereas the lack of D_2O/H_2O exchange observed by *Cziczo et al.* [1997] was on a seconds timescale.) Moreover, as several studies have shown [*Allen et al.*, 1996; *Beichert and Finlayson-Pitts*, 1996; *Fenter et al.*, 1994; *Peters and Ewing*, 1996; *Vogt and Finlayson-Pitts*, 1994], small amounts of water associated with solid salt particles augment the progress of both (R1) and (R2). The fissures of structure III might be reservoirs of this facilitating water. Thus the morphology of aerosol particles can be important to the progress of important heterogeneous chemical reactions. While the composition and structure of sea-salt aerosol particles will be more complex than those of NaCl particles, we anticipate that pockets of water would also be present.

5. Conclusion

IR spectroscopy has been used to determine the structure and water content of submicron NaCl particulates in aerosols at 15–95% RH. Aerosols above 44% RH did not reach equilibrium with the surrounding H_2O vapor during the timescale accessible to these experiments. Presumably, these particulates are in the form of droplets of saturated or supersaturated salt solution. There was a sharp transition in water content near 50% RH consistent with the crystallization of supersaturated NaCl droplets. The NaCl particulates in aerosols below 50% RH had an anomalously large water content as determined by IR photometric measurements. The high water content can be explained by invoking porous NaCl crystalline particulates. The availability of this water in the particulates can contribute to the efficiency of a variety of heterogeneous reactions that can occur in the atmosphere.

Appendix

A1. Calculation of Scattering Spectrum

Briefly, the extinction spectrum as calculated by MIECALC is given by

$$E(\tilde{\nu}) = D_{\text{part}}\left[\sum_{i=0}^{L} \Delta f_i(d_i, \bar{d}, \zeta)[C_{\text{abs}}(d_i, \tilde{\nu}) + C_{\text{sca}}(d_i, \tilde{\nu})]\right] z/2.303 + b. \quad \text{(A1)}$$

Here the lognormal distribution function $f_i(d_i, \bar{d}, \zeta)$ has been divided into $L + 1$ intervals. The functions $C_{\text{abs}}(d_i, \tilde{\nu})$ and $C_{\text{sca}}(d_i, \tilde{\nu})$ are the absorption and scattering cross sections of an individual particle of diameter d_i. These cross sections are calculated from Mie theory using the BHMIE program written by *Bohren and Huffman* [1983]. The quantity z is the path length of the IR cell. The parameter b is an empirical baseline offset constant that is added to correct for multiple scattering and the finite acceptance angle of the detector [*Bohren and Huffman*, 1983].

In a lognormal distribution of diameters the range $\bar{d}\zeta^{-5}$ to $\bar{d}\zeta^{5}$, which encompasses more than 99.9% of the particles, is given by ℓ where

$$\ell = \bar{d}\ \zeta^5 - \bar{d}\zeta^{-5}. \quad \text{(A2)}$$

As in our previous treatment [*Weis and Ewing*, 1996], we divide the distribution into $L + 1$ intervals where L is the integer closest to $S\ell$, and S is a positive integer chosen to produce a number of intervals which adequately approximates the lognormal distribution function. (Here we have used $S = 100$.) The particles in the ith interval are treated as monodisperse with a diameter of

$$d_i = \bar{d}\ \zeta^{-5}e^{i/s}. \quad \text{(A3)}$$

(Equation (A3) corrects two typographical errors that appeared in (17) of our previous paper [*Weis and Ewing*, 1996].) The area under the distribution function between d_i and d_{i+1} may be approximated by

$$\Delta f_i(d_i, \bar{d}, \zeta) = \frac{1}{\sqrt{2\pi}\ln\zeta}\exp\left[-\frac{(\ln d_i - \ln \bar{d})^2}{2\ln^2\zeta}\right]\frac{\ell}{L}. \quad \text{(A4)}$$

The calculation of the absorption and scattering cross sections requires the complex index of refraction of NaCl, $\eta = n + i\kappa$. The real component of the index of refraction of NaCl, n, was obtained by interpolation from data in the AIP Handbook [*Gray*, 1982]; the imaginary component κ was assigned a negligible value of 1×10^{-7} that is an upper limit given by *Toon et al.* [1976].

Removal of the scattering component for particles at low relative humidity involved three steps. First, the lognormal distribution parameters $\bar{d}$ and ζ were fixed and the particle number density and baseline offset D_{part} and b were optimized using a nonlinear least squares regression to fit $E(\tilde{\nu})$ to the experimental spectrum in regions where there was no absorption: 6000–3750, 2900–2400, and 2290–1800 cm^{-1}. Next, the scattering component was calculated over the entire spectral range by setting C_{abs} to zero using the optimized values of D_{part} and b and the fixed values of $\bar{d}$ and ζ. This process was repeated several times as $\bar{d}$ was adjusted by trial and error. The values of $\bar{d}$, ζ, D_{part}, and b, which were used to remove the scattering component from each of the extinction spectra and the phase from which the index of refraction data were taken, are compiled in Table A1.

Table A1. Parameters Used to Fit the Scattering Component of the Extinction Spectrum

Percent RH	$\bar{d}/\mu\text{m}$	ζ	$D_{\text{part}}/10^{12}\ \text{m}^{-3}$	$b/10^{-3}$	Index of Refraction
14	0.23	2.0	5.5	−3.3	crystalline
14	0.23	2.0	5.6	−3.9	crystalline
18	0.21	2.0	8.1	−5.3	crystalline
21	0.23	2.0	5.4	−4.0	crystalline
27	0.23	2.0	6.0	−4.1	crystalline
43	0.23	2.0	5.7	−5.1	crystalline
48	0.23	2.0	5.7	−4.5	crystalline
49	0.30	2.0	8.2	−11	5 M
50	0.30	2.0	8.5	−12	5 M
55	0.23	2.0	8.3	−6.9	crystalline
66	0.30	2.0	17	−21	5 M
87	0.37	2.0	13	−43	5 M
88	0.30	2.0	24	−28	5 M
96	0.40	2.0	15	−49	3 M

Real component of crystalline index of refraction taken from AIP Handbook [*Gray*, 1982]. Imaginary component of crystalline index of refraction taken from *Toon et al.* [1976]. 3 M and 5 M index of refraction data from *Querry et al.* [1972].

A similar procedure was used to extract the absorption from the extinction spectra of the aerosols at high relative humidity. In these cases the complex index of refraction for either 3 M or 5 M NaCl [*Querry et al.*, 1972] was used. A calculated extinction spectrum for given values of $\bar{d}$ and ζ was fit to the experimental spectrum over the range 5000–1300 cm^{-1} by adjusting D_{part} and b (Figure 4, curve B). (The region was not extended to 6000 cm^{-1} as in the low-humidity spectra because the index of refraction data are only available up to 5000 cm^{-1}). Again, trial and error was used to determine the best values of $\bar{d}$ ($\zeta = 2$ was assumed) and also whether to use the 3 M or 5 M complex index of refraction. The parameters required to remove the scattering components from the extinction spectra are tabulated in Table A1.

Although there are discrepancies between the parameters listed in Table A1 and the manufacturer's specifications for the atomizer (for dried particles, $\bar{d} \approx 0.2\ \mu\text{m}$, $\zeta = 2$, and $D_{\text{part}} = 10^{14}\ \text{m}^{-3}$), this is not surprising. As has already been pointed out, Mie theory applies only to homogeneous spheres. In the discussion it is shown that the NaCl particles at low humidity are neither homogeneous nor spherical. At high humidity the use of 3 M or 5 M NaCl solution index of refraction data may not be appropriate since the solute concentration in the particles is not known. Finally, no attempt was made to optimize the fit with respect to the geometric standard deviation parameter ζ. As further calculations show (D. D. Weis and Ewing, manuscript in preparation, 1999), for a broad distribution of diameters such as this, there is not a unique fit to an experimental spectrum, rather many sets of the four parameters $\bar{d}$, ζ, D_{part}, and b can produce equivalent fits to a spectrum; thus the values of these parameters do not necessarily have physical significance. The goal of these calculations was the removal of the scattering component of the spectrum, not an accurate determination of the four parameters. Although an empirical function might also be used to fit the scattering spectrum, the

use of Mie theory conveniently (even if not efficiently) reproduces the form of the scattering spectrum using parameters that can be easily guessed.

A2. Surface Area of Cubic Aggregates

We seek to determine the surface area of a collection of particles that are aggregates of small cubes (structure II in Figure 1) which have a uniform edge length of s^*. We require that the distribution of the mass of solid (or equivalently, its volume) be the same as for a collection of nonporous cubes (structure I in Figure 1). In other words an initial droplet of NaCl solution, when dried, might adopt either structure I or II, but the mass (or volume) of solid NaCl in the particle would be the same as that in the initial droplet. Thus the volume distribution of the two structures, I and II, will be the same, while the surface area distribution would be dramatically different.

For a given edge length s, the volume of a nonporous cube will be s^3 and that of the corresponding aggregate (with the same volume of solute) will be ns^{*3}, where n is the number of cubes in the aggregate. It then follows that

$$n = (s/s^*)^3. \tag{A5}$$

(The implicit restriction that n must be an integer will be overlooked so that n will be permitted to take any positive value.) For any collection of particles, the mean volume $\bar{V}$ is given by

$$\bar{V} = \int_s f(s)v(s)\,ds \tag{A6}$$

where $f(s)$ is the distribution function (e.g., lognormal) of s such that $\int_s f(s)ds \equiv 1$, and $v(s)$ is the volume. For nonporous cubes,

$$\bar{V} = \int_s f(s)s^3\,ds. \tag{A7}$$

For the aggregates, the mean surface area $\bar{a}$ is given by

$$\bar{a} = \int_s f(s)6n(s)s^{*2}\,ds. \tag{A8}$$

By (A5) the mean surface area is also

$$\bar{a} = (6/s^*)\int_s f(s)s^3\,ds. \tag{A9}$$

We have required that the volume distribution of the nonporous cubes and aggregates be the same; thus we may equate (A6) and (A7), so (A9) becomes

$$\bar{a} = 6\bar{V}/s^*. \tag{A10}$$

For a lognormal distribution of diameters, the Hatch-Choate equation [*Hinds*, 1982] relates $\bar{V}$ to $\bar{s}$, so

$$\bar{a} = \frac{6}{s^*}\left(\bar{s}\,\exp\left(\tfrac{3}{2}\ln^2\zeta\right)\right). \tag{A11}$$

The total surface area per unit volume of aerosol ($m^2\ m^{-3}$) $[a]$ is then

$$[a] = D_{\text{part}}\bar{a}. \tag{A12}$$

Acknowledgment. This research has been supported by the National Science Foundation under grant NSF ATM96-31838.

References

Allen, H. C., J. M. Laux, R. Vogt, B. J. Finlayson-Pitts, and J. C. Hemminger, Water-induced reorganization of ultrathin nitrate films on NaCl: Implications for the tropospheric chemistry of sea salt particles, *J. Phys. Chem.*, *100*, 6371–6375, 1996.

Anthony, S. E., R. T. Tisdale, R. S. Disselkamp, and M. A. Tolbert, FTIR studies of low temperature sulfuric acid aerosols, *Geophys. Res. Lett.*, *22*, 1105–1108, 1995.

Barraclough, P. B., and P. G. Hall, The adsorption of water vapour by lithium fluoride, sodium fluoride and sodium chloride, *Surf. Sci.*, *46*, 393–417, 1974.

Beichert, P., and B. J. Finlayson-Pitts, Knudsen cell studies of the uptake of gaseous HNO_3 and other oxides of nitrogen on solid NaCl: The role of surface adsorbed water, *J. Phys. Chem.*, *100*, 15,218–15,228, 1996.

Bertram, A. K., D. D. Patterson, and J. J. Sloan, Mechanisms and temperatures for the freezing of sulfuric acid aerosols measured by FTIR extinction spectroscopy, *J. Phys. Chem.*, *100*, 2376–2383, 1996.

Bohren, C. F., and D. R. Huffman, *Absorption and Scattering of Light by Small Particles*, 530 pp., Wiley-Interscience, New York, 1983.

Bruch, L. W., A. Glebov, J. P. Toennies, and H. Weiss, A helium atom scattering study of water adsorption on the NaCl(100) single crystal surface, *J. Chem. Phys.*, *103*, 5109–5120, 1995.

Cheng, R. J., The generation of secondary marine aerosols: The crystallization of seawater droplets, in *Atmospheric Aerosols and Nucleation*, edited by P. E. Wagner and G. Vali, pp. 589–592, Springer-Verlag, New York, 1988.

Cheng, R. J., D. C. Blanchard, and R. J. Cipriano, The formation of hollow sea-salt particles from the evaporation of drops of seawater, *Atmos. Res.*, *22*, 15–25, 1988.

Clapp, M. L., R. E. Miller, and D. R. Worsnop, Frequency-dependent optical constants of water ice obtained directly from aerosol extinction spectra, *J. Phys. Chem.*, *99*, 6317–6326, 1995.

Cohen, M. D., R. C. Flagan, and J. H. Seinfeld, Studies of concentrated electrolyte solutions using the electrodynamic balance, 3, Solute nucleation, *J. Phys. Chem.*, *91*, 4583–4590, 1987.

Cziczo, D. J., J. B. Nowak, J. H. Hu, and J. P. D. Abbatt, Infrared spectroscopy of model tropospheric aerosols as a function of relative humidity: Observation of deliquescence and crystallization, *J. Geophys. Res.*, *102*, 18,843–18,850, 1997.

Dai, D. J., S. J. Peters, and G. E. Ewing, Water adsorption and dissociation on NaCl surfaces, *J. Phys. Chem.*, *99*, 10,299–10,304, 1995.

Davies, J. A., and R. A. Cox, Kinetics of the heterogeneous reaction of HNO_3 with NaCl: Effect of water vapor, *J. Phys. Chem., Ser. A*, *102*, 7631–7642, 1998.

Downing, H. E., and D. Williams, Optical constants of water in the infrared, *J. Geophys. Res.*, *80*, 1656–1661, 1975.

Ewing, G. E., and S. J. Peters, Adsorption of water on NaCl, *Surf. Rev. Lett.*, *4*, 757–770, 1997.

Fenter, F. F., Heterogeneous kinetics of N_2O_5 uptake on salt, with a systematic study of the role of the surface presentation (for N_2O_5 and HNO_3), *J. Phys. Chem.*, *100*, 1008–1019, 1996.

Fenter, F. F., F. Caloz, and M. Rossi, Kinetics of nitric acid uptake by salt, *J. Phys. Chem.*, *98*, 9801–9810, 1994.

Folsch, S., and M. Henzler, Water adsorption on the NaCl surface, *Surf. Sci.*, *247*, 269–273, 1991.

Fölsch, S., A. Stock, and M. Henzler, Two-dimensional water condensation of the NaCl(100) surface, *Surf. Sci.*, *264*, 65–72, 1992.

Foster, M., and G. E. Ewing, Infrared spectroscopic study of water thin films on NACl (100), *Surf. Sci.*, *427–428*, 102–108, 1999.

Gray, D. E. (Ed.), *American Institute of Physics Handbook*, 3rd ed., McGraw-Hill, New York, 1982.

Hinds, W. C., *Aerosol Technology: Properties, Behavior, and Measurement of Airborne Particles*, 424 pp., Wiley-Interscience, New York, 1982.

Horn, A. B., T. Koch, M. A. Chesters, M. R. S. McCoustra, and J. R. Sodeau, A low-temperature infrared study of the reactions of stratospheric NO_y reservoir species dinitrogen pentoxide with water ice, 80–160K, *J. Phys. Chem.*, *98*, 946–951, 1994.

Leong, K. H., Morphological control of particles generated from the evaporation of solution droplets: Theoretical considerations, *J. Aerosol Sci.*, *18*, 511–524, 1987.

Linde, D. R. (Ed.), *Handbook of Chemistry and Physics*, 79th ed., CRC Press, Boca Raton, Fla., 1998.

Liu, B. Y. H., Standardization and calibration of aerosol instruments, in *Fine Particles: Aerosol Generation, Measurement, Sampling, and Analysis*, edited by B. Y. H. Liu, pp. 40–53, Academic, San Diego, Calif., 1976.

Mudd, H. T., Jr., C. H. Kruger, and E. R. Murray, Measurement of IR backscatter spectra from sulfuric acid and ammonium sulfate aerosols, *Appl. Opt.*, *21*, 1146–1154, 1982.

Perry, R. J., A. J. Hunt, and D. R. Huffman, Experimental determinations of Mueller scattering matrices for nonspherical particles, *Appl. Opt.*, *17*, 2700–2710, 1978.

Peters, S. J., and G. E. Ewing, Reaction of NO_2(g) with NaCl(100), *J. Phys. Chem.*, *100*, 14,093–14,102, 1996.

Peters, S. J., and G. E. Ewing, Thin film water on NaCl(100) under ambient conditions: An infrared study, *Langmuir*, *13*, 6345–6348, 1997a.

Peters, S. J., and G. E. Ewing, Water on salt: An infrared study of adsorbed H_2O on NaCl(100) under ambient conditions, *J. Phys. Chem., Ser. B*, *101*, 10,880–10,886, 1997b.

Pinnick, R. G., and H. J. Auvermann, Response characteristics of Knollenberg light-scattering aerosol counters, *J. Aerosol Sci.*, *10*, 55–74, 1979.

Querry, M. R., R. C. Waring, W. E. Holland, G. M. Hale, and W. Nijm, Optical constants in the infrared for aqueous solutions of NaCl, *J. Opt. Soc. Am.*, *62*, 849–855, 1972.

Robbins, R. C., R. D. Cadle, and D. L. Eckhardt, The conversion of sodium chloride to hydrogen chloride in the atmosphere, *J. Meteorol.*, *16*, 53–56, 1959.

Tang, I. N., and H. R. Munkelwitz, Simultaneous determination of refractive index and density of an evaporating aqueous solution droplet, *Aerosol Sci. Technol.*, *15*, 210–207, 1991.

Tang, I. N., K. H. Fung, D. G. Imre, and H. R. Munkelwitz, Phase transformation and metastability of hygroscopic microparticles, *Aerosol Sci. Technol.*, *23*, 443–453, 1995.

Taylor, D. P., W. P. Hess, and M. I. McCarthy, Structure and energetics of the water/NaCl(100) interface, *J. Phys. Chem., Ser. B*, *101*, 7455–7463, 1997.

Timonen, R. S., L. T. Chu, M.-T. Leu, and L. F. Keyser, Heterogeneous reaction of $ClONO_2$(g) + NaCl(s) → Cl_2(g) + $NaNO_3$(s), *J. Phys. Chem.*, *98*, 9509–9517, 1994.

Toon, O. B., J. B. Pollack, and B. N. Khare, The optical constants of several atmospheric aerosol species: Ammonium sulfate, aluminum oxide, and sodium chloride, *J. Geophys. Res.*, *81*, 5733–5748, 1976.

van de Hulst, H. C., *Light Scattering by Small Particles*, 470 pp., John Wiley, New York, 1957.

Vogt, R., and B. J. Finlayson-Pitts, A diffuse reflectance infrared Fourier transform spectroscopic (DRIFTS) study of the surface reaction of NaCl with gaseous NO_2 and HNO_3, *J. Phys. Chem.*, *98*, 3747–3755, 1994.

Warneck, P., *Chemistry of the Natural Atmosphere*, 753 pp., Academic, San Diego, Calif., 1988.

Wasserman, B., S. Mirbt, J. Reif, J. C. Zink, and E. Matthias, Clustered water adsorption on the NaCl(100) surface, *J. Chem. Phys.*, *98*, 10,049–10,060, 1993.

Weis, D., Infrared spectroscopy of aerosols: Theory, techniques, and applications, Ph.D. dissertation, Indiana Univ., Bloomington, 1998.

Weis, D. D., and G. E. Ewing, Infrared spectroscopic signatures of $(NH_4)_2SO_4$ aerosols, *J. Geophys. Res.*, *101*, 18,709–18,720, 1996.

Weis, D. D., and G. E. Ewing, Infrared spectroscopy of tropospheric aerosols, *Glas. Hem. Technol. Maked*, *16*, 3–10, 1997.

Weis, D. D., and G. E. Ewing, Absorption anomalies in ratio and subtraction FT-IR spectroscopy, *Anal. Chem.*, *70*, 3175–3183, 1998.

G. E. Ewing (corresponding author), Department of Chemistry, Indiana University, Bloomington, IN 47405.

D. D. Weis, Department of Chemistry and Biochemistry, Middlebury College, Middlebury VT 05753. (dweis@middlebury.edu.)

(Received September 14, 1998; revised April 12, 1999; accepted April 20, 1999.)